Supporting Information

Multifunctional MgAl LDH/Zn-MOF S-scheme heterojunction: efficient hydrogen production, methyl red removal, and CO_2 adsorption

Ihsan Maseeh[¥a], Farheen Anwar[¥a], Sadia Aroob[a], Tariq Javed[b], Ismat Bibi[a], Afaf Almasoudi[c], Ahmad Raheel[d], Muhammad Arshad Javid[e], Sónia A. C. Carabineiro[f], Muhammad Babar Taj*[a]

[a] Institute of Chemistry, The Islamia University of Bahawalpur, Bahawalpur 63100, Pakistan

[b] Department of Chemistry, University of Sahiwal, Sahiwal 57000, Pakistan

[c] Chemistry Department, Faculty of Science, King Abdulaziz University, P.O. Box 42734, Jeddah, Saudi Arabia

[d] Department of Chemistry, Quaid-e-Azam University, Islamabad 44000, Pakistan

[e] Institute of Physics, The Islamia University Bahawalpur, Bahawalpur 63100, Pakistan

[f] LAQV-REQUIMTE, Department of Chemistry, NOVA School of Science and Technology, Universidade NOVA de Lisboa, 2829-516 Caparica, Portugal

[¥]Both authors have equal contributions, so they are considered first authors.

***Corresponding authors: dr.taj@iub.edu.pk (M.B.T.)

Section S1

1. Kinetic studies

For the kinetic studies, 25 ml of MR dye solution was placed in a flask, followed by the addition of 25 mg of MgAl LDH/Zn-MOF adsorbent. The mixture was continuously stirred for 4 h, and samples were collected at 20-min intervals to measure the concentration of the dye solution. To study the adsorption kinetics, the experimental data was fitted to various kinetic models, including pseudo-first-order kinetics, Eq. 1[1, 2], pseudo-second-order kinetics, Eq. 2[2, 3], liquid-film diffusion model, Eq. 3[4], and intra-particle diffusion model, Eq. 4[4] as follows:

$K_1 = \ln q_e – \ln(q_e\text{-}q_t)/t$ (1)

Where t is the adsorption time, q_e is the adsorption capacity at equilibrium (mg/g), q_t is the adsorption capacity at time t (mg/g), K_1 is the rate constant for pseudo-first-order kinetics (h^{-1}). The data can be plotted as ln (q_e-q_t) vs time.

$K_2 = q_t/t\ (1/q_e2 + t/q_e)$ (2)

K_2 is the rate constant for the pseudo-second-order kinetics (g mg^{-1} h^{-1}). For this model, the data can be plotted as t/q_t vs time.

$K_f = A – \ln(1\text{-}\ q_t/q_e)/t$ (3)

K_f is the rate constant for the liquid-film diffusion model (h^{-1}). The data can be plotted as ln (1– q_e/q_t) vs time.

$K_d = q_t – C/t_{0.5}$ (4)

K_d is the rate constant for the intra-particle diffusion model ($g.mg^{-1}h^{-0.5}$). For this, data can be plotted as $q_t/t_{0.5}$ for this model.

2. Isotherm Models

After analysis of the kinetics mechanisms, various isothermal models were applied to the data, including the Langmuir (Eq. 5)[4], Freundlich (Eq. 6)[5], and Temkin (Eq. 7)[6] models.

The Langmuir model describes the adsorption process of a monolayer of molecules onto a surface with a limited number of identical sites. This model assumes that the adsorption occurs at specific homogeneous sites within the absorbent and that there is no transmigration of the adsorbate in the plane of the surface. The Langmuir equation is given by:

$$C_e/q_e = C_e/q_{max} + 1/q_{max} K_L \qquad (5)$$

Here, C_e is the equilibrium concentration of adsorbate (mg/l), q_e is the equilibrium adsorption capacity (mg/g), qmax is the maximum adsorption capacity (mg/g), and K_L is the Langmuir adsorption constant (l/mg). A plot of C_e/q_e vs C_e is used to evaluate the Langmuir model.

The Freundlich model is a semi-empirical isotherm model that describes the adsorption process onto heterogeneous surfaces. The Freundlich equation is given as follows:

$$\ln q_e = 1/n \ln C_e + \ln K_F \qquad (6)$$

Here, K_F is the Freundlich adsorption constant, and n is the Freundlich exponent, which characterizes the heterogeneity of the adsorbent surface. A plot of $\ln q_e$ vs $\ln C_e$ is used to evaluate the Freundlich model.

The Temkin model assumes that the heat of adsorption of all the molecules in the layer decreases linearly with coverage due to adsorbent-adsorbate interactions. The Temkin equation is given as follows:

$$q_e = K_T \ln C_e + K_T \ln f \qquad (7)$$

Here, K_T is the Temkin binding constant (l/mg), and f is the Temkin isotherm constant related to the heat of adsorption. A q_e vs $\ln C_e$ plot is used to evaluate the Temkin model.

3. Thermodynamic Study

The thermodynamic study was conducted at different temperatures (303 K, 313 K, 323 K, 333 K and 343 K) by adding 25 mg of adsorbent to 25 ml of MR dye solution (5×10^{-5} M) and stirring continuously for 3 h. Various thermodynamic parameters were calculated using the following equations (8-10).

$$\Delta G_o = -RT \ln K_L \qquad (8)$$

$$\Delta H_o = -\text{slope} \times R \qquad (9)$$

$$\Delta S_o = -\text{intercept} \times R \qquad (10)$$

Here, ΔG_o represents the change in Gibbs free energy (kJ/mol), R is the universal gas constant with a value of 8.314 J/mol.K, T is the absolute temperature (K), K_L is the equilibrium constant, ΔS_o represents the change in entropy (kJ/mol.K), and ΔH_o represents the change in enthalpy (kJ/mol)

Figures:

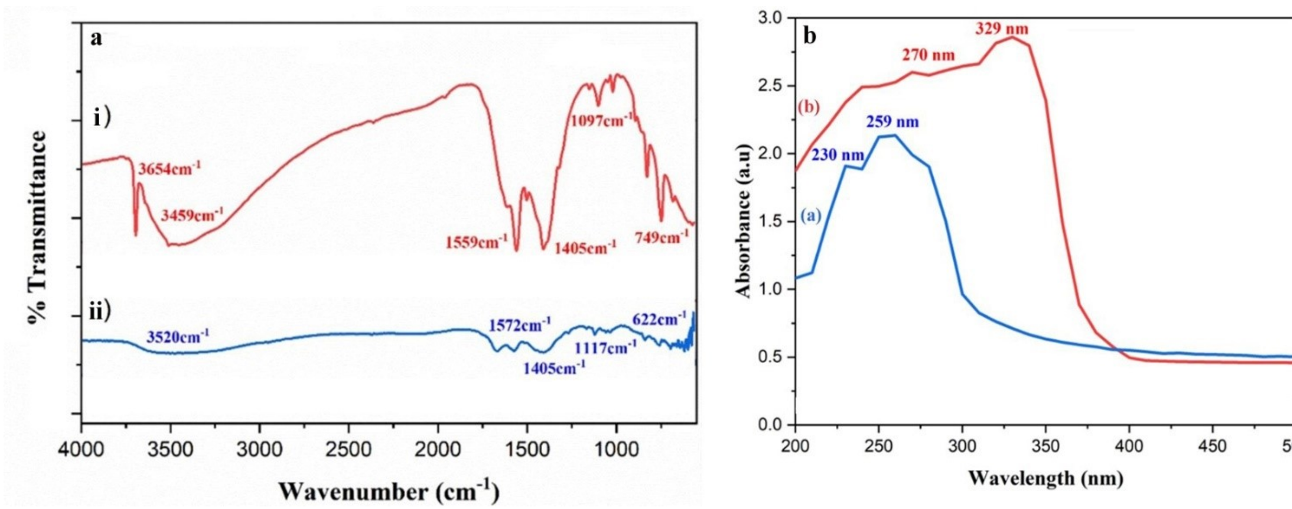

Figure S1: (a) FTIR spectra of the prepared (i) MgAl LDH and (ii) MgAl-LDH/Zn-MOF samples, **(b)** UV-vis spectra of the prepared (i) MgAl LDH and (ii) MgAl-LDH/Zn-MOF samples.

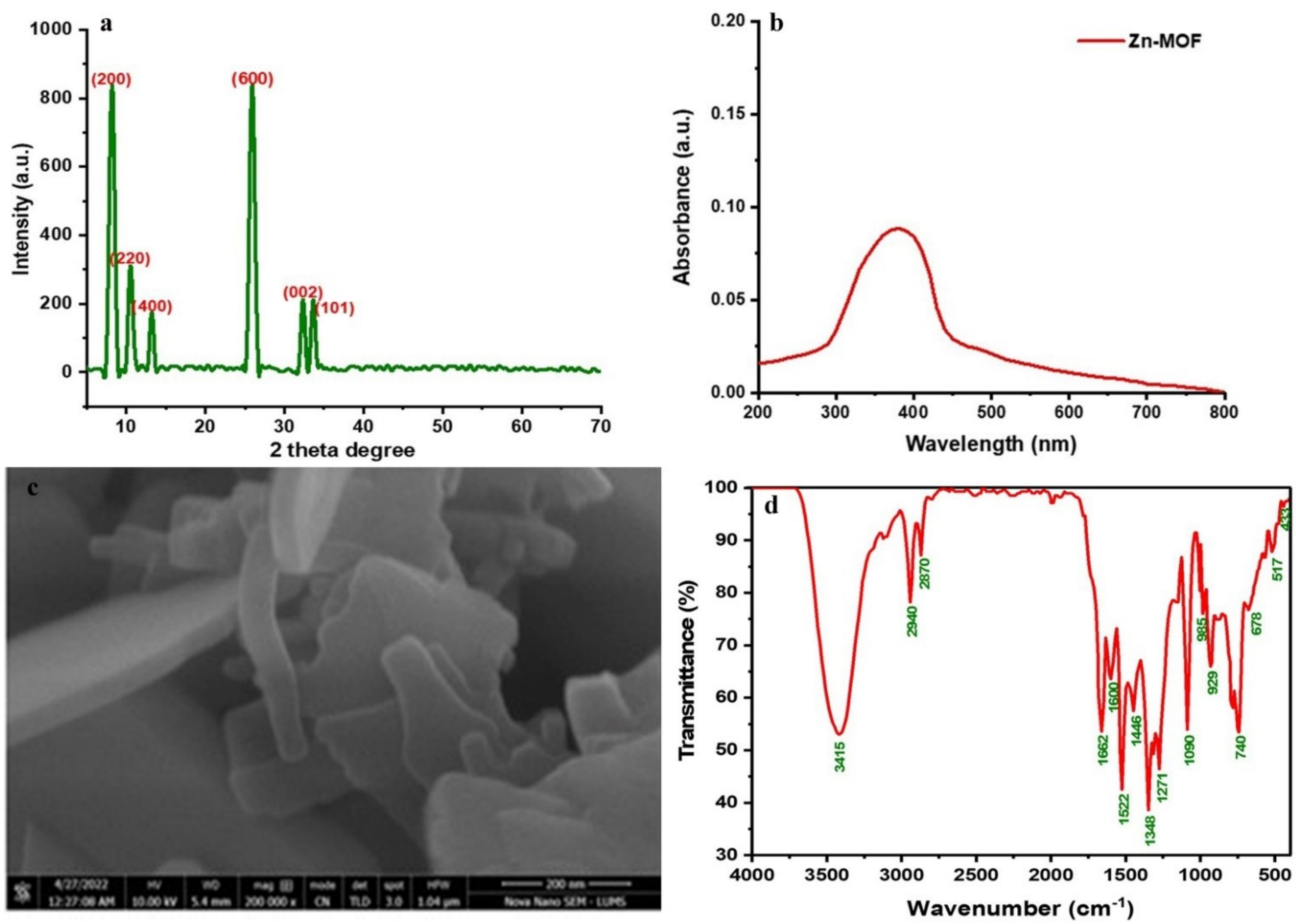

Figure S2: (a) PXRD spectrum **(b)** UV-vis spectrum **(c)** SEM image, and **(d)** FTIR spectrum of Zn-MOF.

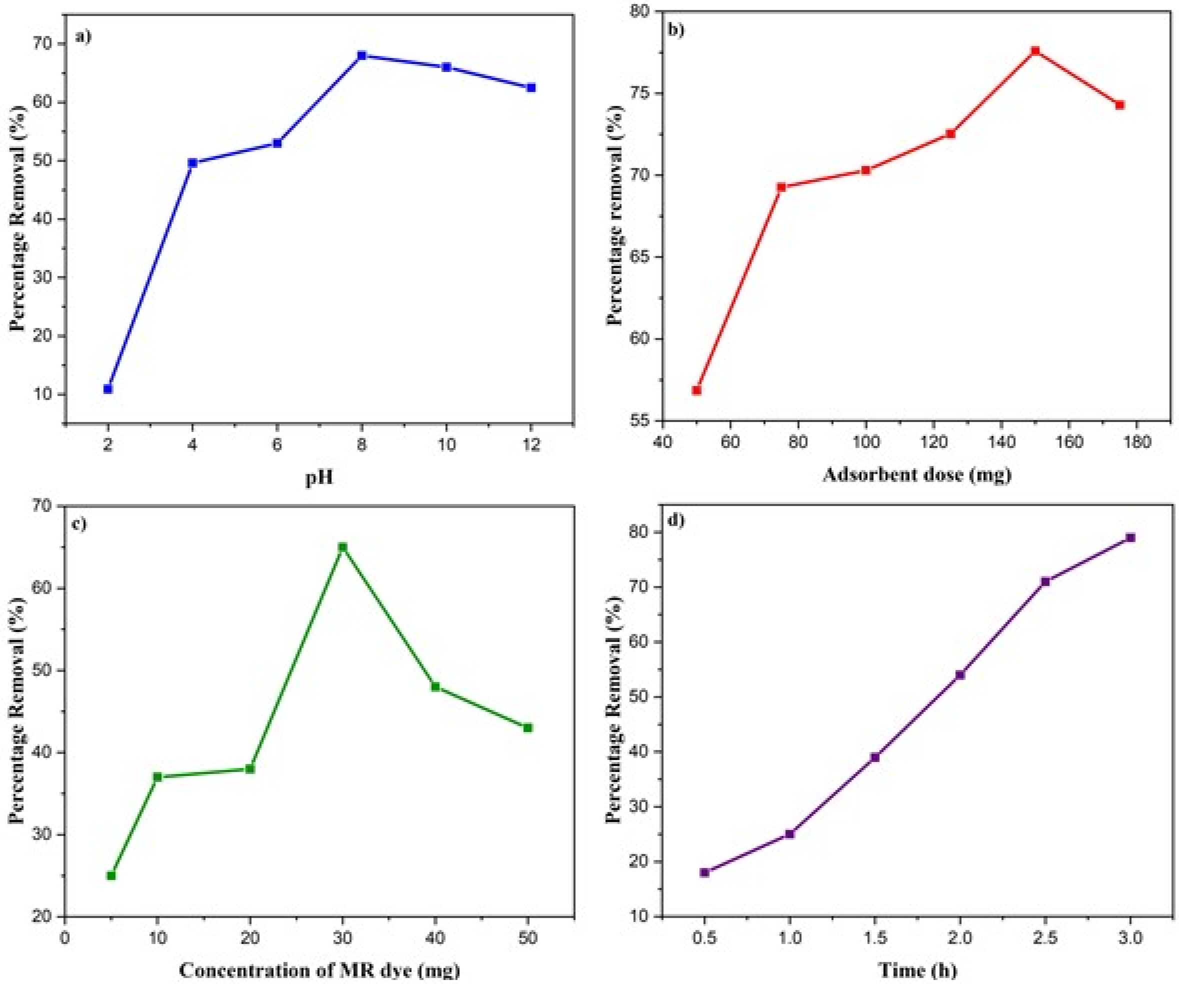

Figure S3: Comparative graphs for adsorption of MR dye at different (a) pH, (b) adsorbent dose, (c) concentration of dye, and (d) time.

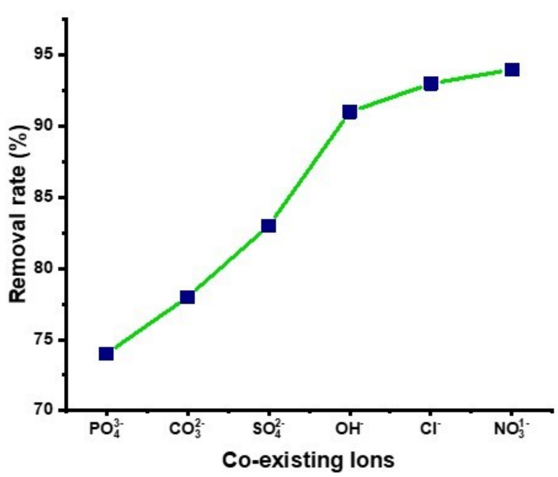

Figure S4: Effect of co-existing ions in the removal of MR dye.

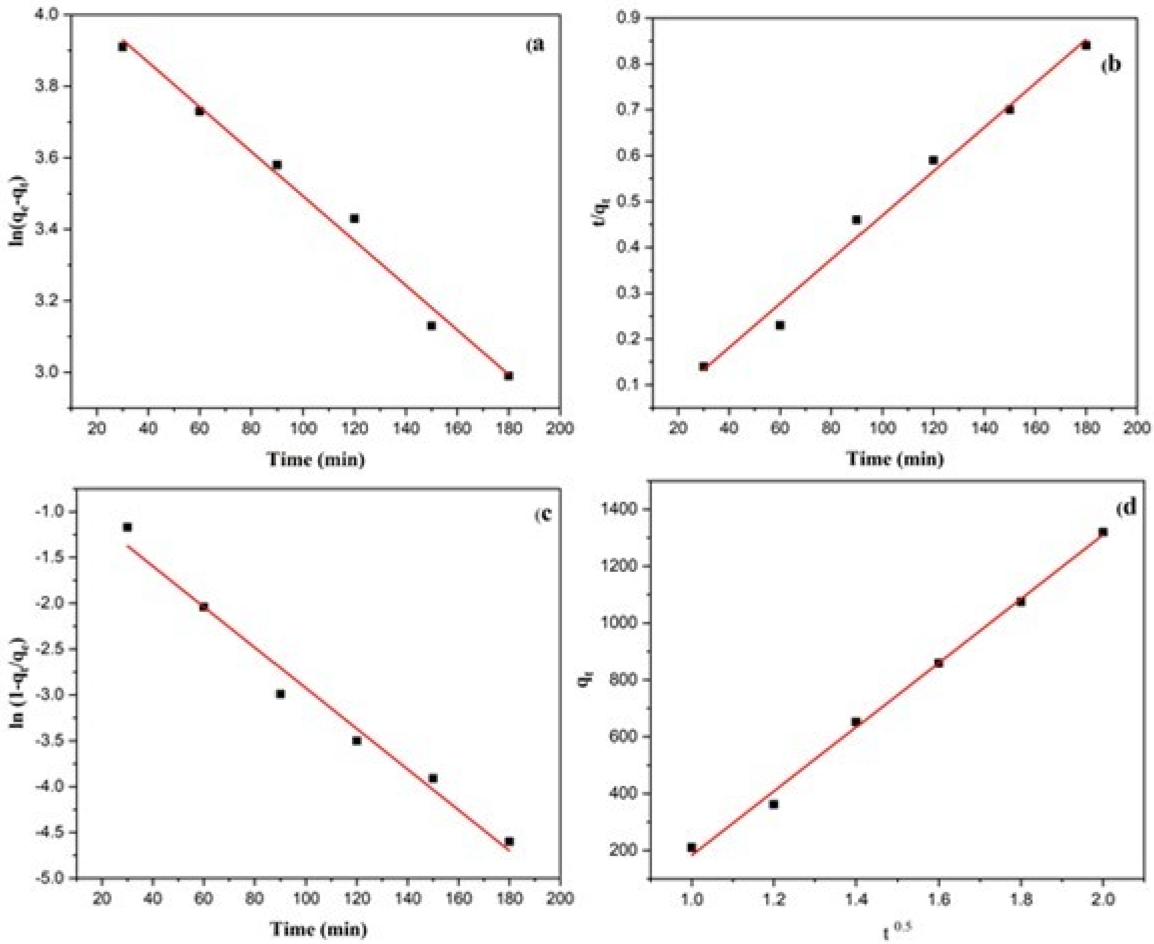

Figure S5: Kinetic models for the adsorption of MR dye on MgAl LDH/Zn-MOF (a) pseudo-first order kinetics, (b) pseudo-second-order kinetics, (c) liquid-film diffusion model, and (d) intra-particle diffusion model.

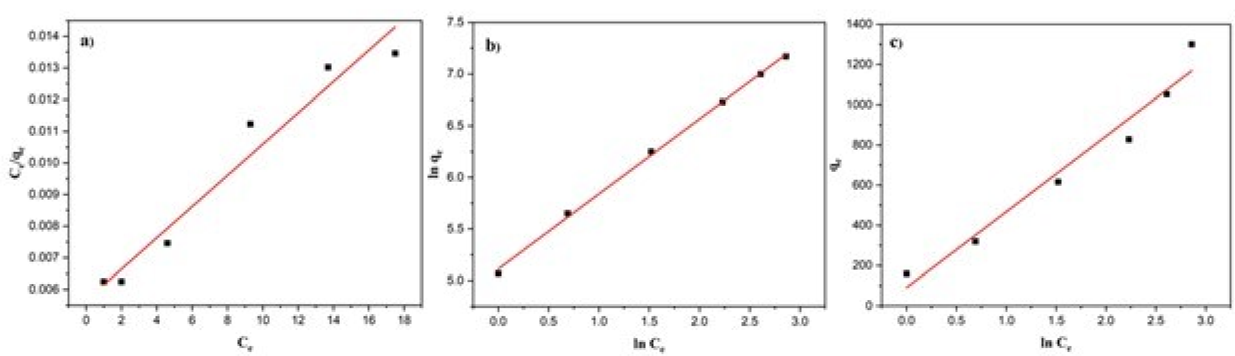

Figure S6: Adsorption isotherms for MR dye on MgAl LDH/Zn-MOF (a) Langmuir, (b) Freundlich, and (c) Temkin models.

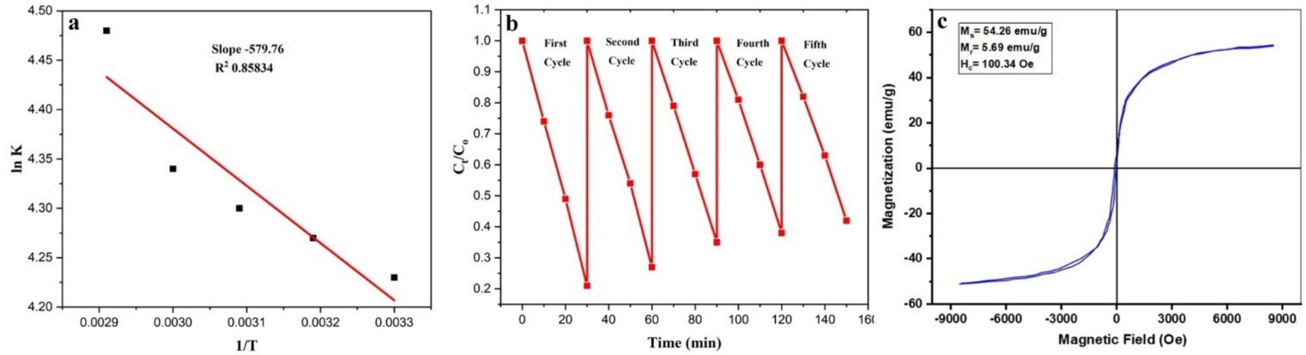

Figure S7: (a) Plot between ln K and 1/T for the thermodynamic study of adsorption **(b)** Reusability of MgAl LDH/Zn-MOF in the cyclic removal of MR dye under adsorption conditions: pH = 8, $C_o = 5\times10^{-5}$ M, T = 25 °C, and t = 150 min, **(c)** VSM analysis of the MgAl LDH/Zn-MOF.

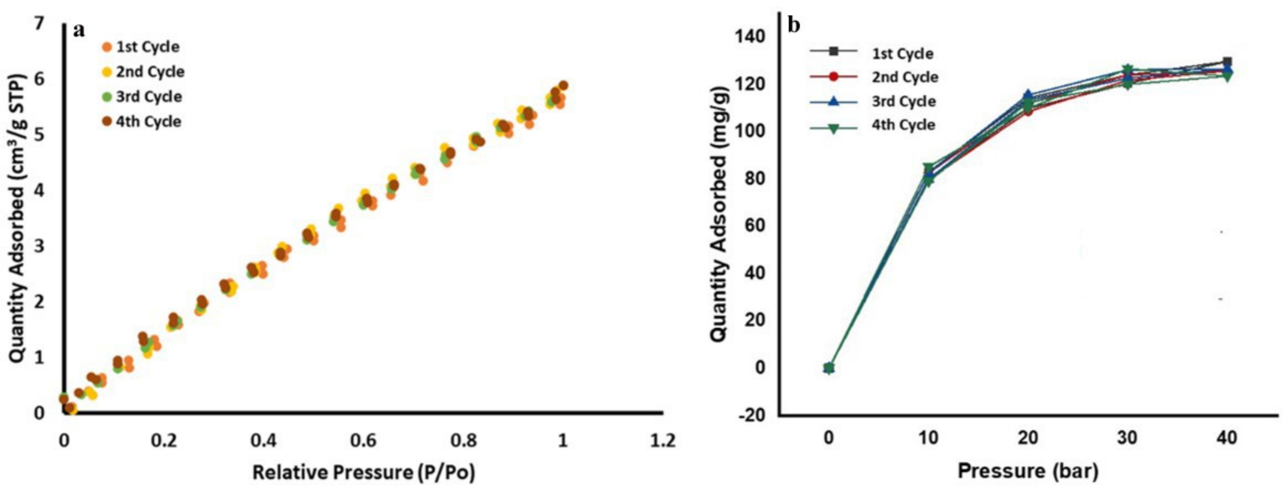

Figure S8:. (a) Cyclic adsorption isotherms up to 1 bar at 25 °C and **(b)** the cyclic CO_2 uptake of MgAl LDH/Zn-MOF at high pressure of 40 bar.

Tables

Table S1: Comparison of the hydrogen production rate of MgAl LDH/Zn-MOF with other MOFs in the literature.

Photocatalyst	Sacrificial reagent	Irradiation source	H_2 production rate	Reference
MgAl LDH/Zn-MOF	10 vol% triethanolamine	direct solar irradiation	23000 µmol g^{-1} h^{-1}	Present study
MOF-199/Ni	---	300 W Xe lamp	24 400 µmol h^{-1} g^{-1}	[7]
MgAl-LDH coupled with CoSx	10 vol% triethanolamine	simulated sunlight irradiation	263 µmol g^{-1} h^{-1}	[8]
ZIF-67@NiAl LDH	15 vol% triethanolamine	5W LED	2900 µmol g^{-1} h^{-1}	[9]
CoAl LDH@ Ni-MOF-74	15 vol% triethanolamine	5W LED	213 µmol g^{-1} h^{-1}	[10]
Co-Ru@MOF	---	---	15,144 ml min^{-1} g^{-1}	[11]
MIL-167/MIL-125-NH_2	10 ml triethylamine	visible light	455 µmol g^{-1} h^{-1}	[12]
Pt(4.38 wt%)/CuII-MOF	5 ml triethylamine	300 W Xe lamp	2.51 µmol g^{-1} h^{-1}	[13]
Cu-MOF/CeO_2	---	electrochemical	97.9 µg ml^{-1}	[14]
Pt/PCN-777	benzylamine	light irradiation	568 µmol g^{-1} h^{-1}	[15]
g-C3N4/ZIF-67	lactic acid	visible light	3329 µmol g^{-1} h^{-1}	[16]
Ni/Cu-BTC	methanol	visible light	200 mmol.h^{-1}	[17]

Table S2. Comparative study for adsorption of MR dye on different adsorbents.

Nanocomposites	Preparation Method	Dye	Removal Rate	References
MgAl LDH/Zn-MOF	Co-precipitation followed by hydrothermal	MR	97%	Current Study
NaAlg-g-CHIT/nZVI	Co-precipitation	MR	66%	[18]
bentonite / chitosan	Precipitation	MR	96%	[19]
NiO@HT-derived C	Precipitation	MR	94%	[20]
MgFe2O4/polyaniline	Co-precipitation	MR	90%	[21]
Ag@Fe nanocomposite	Co-precipitation	MR	93%	[22]
α-MnO2/PANI hybrid	Polymerization	MR	95%	[23]
CuO-HNT	Calcination	MR	98%	[24]

Table S3. Kinetic values for pseudo-first-order kinetics, pseudo-second-order kinetics, liquid-film diffusion, and intra-particle diffusion models.

Parameters	Pseudo-First Order Kinetics	Pseudo-Second Order Kinetics	Liquid Film Diffusion Model	Intra particle Diffusion Model
R^2	0.988	0.987	0.979	0.996
Kinetic Constant	K_1=0.7	K_2=330.99	K_f=9.80	K_d=84.88

Table S4. Isothermal parameters for Langmuir, Freundlich, and Temkin models.

Parameters	**Langmuir Model**	**Freundlich Model**	**Temkin Model**
R^2	0.998	0.957	0.952
Kinetic Constant	K_L=1.05	K_F=0.71	K_T=1746.75

Table S5. Thermodynamic parameters for adsorption of MR dye on MgAl LDH/Zn-MOF.

Dye	**Temperature (K)**	K_L (L mg^{-1})	**ΔG (kJmol^{-1}K)**	**ΔH (kJmol^{-1})**	**ΔS (kJmol^{-1}K)**	R^2
MR	303	69.24	-11286.16	4893.97	50.88	0.8438
	313	71.61				
	323	74.28				
	333	76.78				
	343	89.03				

Table S6. Comparison of CO_2 uptake of MgAl LDH/Zn-MOF with other MOFs in the literature

Material	**BET surface area (m^2 g^{-1})**	**CO_2 uptake**	**References**
MgAl LDH/Zn-MOF	60	129 mgg^{-1}	Current study
[BMPyr][Cl]/AlTp	578.35	68.27 mgg^{-1}	25
Zn-MOF	---	145 mgg^{-1}	26
$MgCl_2$-MOF-74	928	7.8 $mmolg^{-1}$	27
Cu-TDPAT	1938	132 cm^3g^{-1}	28
MOP-(Cu II)	--	121 $mmolg^{-1}$	29
Mg/DOBDC	--	250 mgg^{-1}	30
Ni/DOBDC	--	2.4 $mmolg^{-1}$	31
ZIF-8/PAN-90	888	130 mgg^{-1}	32
IRMOF-74	2440	3.2 $mmolg^{-1}$	33
Mg-MOF-74 -TEPA	1628	26.9 wt%	34
GO@MOF-505	1279	3.94 $mmolg^{-1}$	35
GrO@Cu-BTC	1677	8.19 $mmolg^{-1}$	36

References

1. S. Li, X. Zhang and Y. Huang, *Journal of hazardous materials*, 2017, **321**, 711-719.
2. Y. Sun, X. Wang, W. Song, S. Lu, C. Chen and X. Wang, *Environmental science: nano*, 2017, **4**, 222-232.
3. M. A. Afzal, M. Javed, S. Aroob, T. Javed, M. M. Alnoman, W. Alelwani, I. Bibi, M. Sharif, M. Saleem and M. Rizwan, *Nanomaterials*, 2023, **13**, 2079.
4. S. Zhu, S. Jiao, Z. Liu, G. Pang and S. Feng, *Environmental science: nano*, 2014, **1**, 172-180.
5. S. Aroob, S. A. Carabineiro, M. B. Taj, I. Bibi, A. Raheel, T. Javed, R. Yahya, W. Alelwani, F. Verpoort and K. Kamwilaisak, *Catalysts*, 2023, **13**, 502.
6. S. Aroob, M. B. Taj, S. Shabbir, M. Imran, R. H. Ahmad, S. Habib, A. Raheel, M. N. Akhtar, M. Ashfaq and M. Sillanpää, *Journal of Environmental Chemical Engineering*, 2021, **9**, 105590.
7. J. Zhao, Y. Wang, J. Zhou, P. Qi, S. Li, K. Zhang, X. Feng, B. Wang and C. Hu, *Journal of Materials Chemistry A*, 2016, **4**, 7174-7177.
8. X. Liu, J. Xu, L. Ma, Y. Liu and L. Hu, *Chemical Physics Letters*, 2021, **784**, 139124.
9. K. Wang, S. Liu, Y. Li, G. Wang, M. Yang and Z. Jin, *Applied Surface Science*, 2022, **601**, 154174.
10. Z. Jin, Y. Li and Q. Ma, *Transactions of Tianjin University*, 2021, **27**, 127-138.

11. E. Onat, S. Cevik, Ö. Şahin, S. Horoz and M. S. Izgi, *Journal of the Australian Ceramic Society*, 2021, **57**, 1389-1395.
12. S. Kampouri, F. M. Ebrahim, M. Fumanal, M. Nord, P. A. Schouwink, R. Elzein, R. Addou, G. S. Herman, B. Smit and C. P. Ireland, *ACS Applied Materials & Interfaces*, 2021, **13**, 14239-14247.
13. L. Li, Y. Zhao, Q. Wang, Z.-Y. Liu, X.-G. Wang, E.-C. Yang and X.-J. Zhao, *Inorganic Chemistry Frontiers*, 2021, **8**, 3556-3565.
14. S. Kumaraguru, R. Nivetha, K. Gopinath, E. Sundaravadivel, B. O. Almutairi, M. H. Almutairi, S. Mahboob, M. Kavipriya, M. Nicoletti and M. Govindarajan, *Journal of Materials Research and Technology*, 2022, **18**, 1732-1745.
15. H. Liu, C. Xu, D. Li and H. L. Jiang, *Angewandte Chemie*, 2018, **130**, 5477-5481.
16. K. Devarayapalli, S. P. Vattikuti, T. Sreekanth, K. S. Yoo, P. Nagajyothi and J. Shim, *Applied Organometallic Chemistry*, 2020, **34**, e5376.
17. A. S. Morshedy, H. M. Abd El Salam, A. M. El Naggar and T. Zaki, *Energy & Fuels*, 2020, **34**, 11660-11669.
18. J. K. Adusei, E. S. Agorku, R. B. Voegborlo, F. K. Ampong, B. Y. Danu and F. A. Amarh, *Scientific African*, 2022, **17**, e01273.
19. P. Xiang, C. Deng, L. Liu and Y. Huang, 2020.
20. A. S. Ahmed, M. M. Sanad, A. Kotb, A. N. Negm and M. H. Abdallah, *Materials Advances*, 2023, **4**, 2981-2990.
21. P. Das and A. Debnath, *Journal of Dispersion Science and Technology*, 2023, **44**, 2587-2598.
22. Z. Zaheer, A.-A. Aisha and E. S. Aazam, *Journal of Molecular Liquids*, 2019, **283**, 287-298.
23. Y. Dessie, S. Tadesse and Y. Adimasu, *Chemical Engineering Journal Advances*, 2022, **10**, 100283.
24. Z. U. Zango, N. H. H. Abu Bakar, W. L. Tan and M. A. Bakar, *Journal of Dispersion Science and Technology*, 2018, **39**, 148-154.
25. N. Noorani and A. Mehrdad, *Scientific Reports*, 2023, **13**, 3227.
26. N. Daud, *Materials Today: Proceedings*, 2023.
27. H. An, W. Tian, X. Lu, H. Yuan, L. Yang, H. Zhang, H. Shen and H. Bai, *Chemical Engineering Journal*, 2023, 144052.
28. B. Li, Z. Zhang, Y. Li, K. Yao, Y. Zhu, Z. Deng, F. Yang, X. Zhou, G. Li and H. Wu, *Angewandte Chemie International Edition*, 2012, **51**, 1412-1415.
29. A. López-Olvera, E. Sánchez-González, A. Campos-Reales-Pineda, A. Aguilar-Granda, I. A. Ibarra and B. Rodríguez-Molina, *Inorganic Chemistry Frontiers*, 2017, **4**, 56-64.
30. A. O. Yazaydın, R. Q. Snurr, T.-H. Park, K. Koh, J. Liu, M. D. LeVan, A. I. Benin, P. Jakubczak, M. Lanuza and D. B. Galloway, *Journal of the American Chemical Society*, 2009, **131**, 18198-18199.
31. C. P. Cabello, P. Rumori and G. T. Palomino, *Microporous and Mesoporous Materials*, 2014, **190**, 234-239.
32. Z. Li, Z. Cao, C. Grande, W. Zhang, Y. Dou, X. Li, J. Fu, N. Shezad, F. Akhtar and A. Kaiser, *RSC advances*, 2022, **12**, 664-670.
33. A. M. Fracaroli, H. Furukawa, M. Suzuki, M. Dodd, S. Okajima, F. Gándara, J. A. Reimer and O. M. Yaghi, *Journal of the American Chemical Society*, 2014, **136**, 8863-8866.
34. X. Su, L. Bromberg, V. Martis, F. Simeon, A. Huq and T. A. Hatton, *ACS applied materials & interfaces*, 2017, **9**, 11299-11306.
35. Y. Chen, D. Lv, J. Wu, J. Xiao, H. Xi, Q. Xia and Z. Li, *Chemical Engineering Journal*, 2017, **308**, 1065-1072.
36. W. Huang, X. Zhou, Q. Xia, J. Peng, H. Wang and Z. Li, *Industrial & Engineering Chemistry Research*, 2014, **53**, 11176-11184.